



Thermal Performance Evaluation of a Channel Installed with Inclined-Baffle Turbulators

A. Phila¹ · S. Eiamsa-ard¹ · C. Thianpong²

Received: 10 January 2019 / Accepted: 5 August 2019 / Published online: 20 August 2019
© King Fahd University of Petroleum & Minerals 2019

Abstract

This study shed light on how heat transfer in a rectangular channel can be significantly enhanced by integrating it with inclined baffles. Experiments were performed to investigate the effect of the inclined baffles at different attack angles (θ) of 0° up to 165° in 15° incremental steps. The pitch length (between the consecutive baffles) to baffle height ratio (P/e) and the baffle height to channel height ratio (e/H) remained constant at 10 and 0.15, respectively. Experiments on a channel without baffles and one with typical transverse baffles ($\theta=90^\circ$) were also conducted for comparison. Temperatures measured by the thermochromic liquid crystal image processing technique were employed for plotting the temperature contours on the heated surface. The Reynolds number associated with turbulent flow varied from 9000 to 24,000 under a constant wall heat flux scenario. The heat transfer and pressure drop were characterized by the Nusselt number (Nu) and friction factor (f), respectively. The results showed a promising ability of the inclined baffles to improve the heat transfer rate in the channel, however, this came at the price of an increased pressure drop in the system. The impact of the attack angle on heat transfer and thermal efficiency showed that a 60° attack angle was superior to other attack angles. The results were comparable to those for a 120° attack angle. Additionally, this attack angle enabled the system to accomplish a zenith thermal enhancement factor (η) of 1.11 at a Reynolds number of 9000.

Keywords Heat exchanger · Heat transfer enhancement · Inclined baffle · Rectangular channel

List of Symbols

a	Total height of clearance (m)	H	Channel height (m)
A	Area (m^2)	I	Current (A)
c	Detached clearance (m)	k	Thermal conductivity ($W m^{-1} K^{-1}$)
c/a	Detached-clearance ratio	l	Baffle width (m)
C	Specific heat ($J kg^{-1} K^{-1}$)	L	Channel length (m)
D	Diameter (m)	\dot{m}	Mass flow rate ($kg s^{-1}$)
e	Baffle height (m)	Nu	Nusselt number
e/H	Baffle height to channel height ratio	P	Pitch length (m)
f	Friction factor	P/e	Pitch length to baffle height ratio
h	Convective heat transfer coefficient ($W m^{-2} K^{-1}$)	P/H	Baffle pitch spacing ratio
		ΔP	Pressure drop (Pa)
		Pr	Prandtl number
		q	Heat flux ($W m^{-2}$)
		Q	Heat transfer (W)
		Re	Reynolds number
		s/w	Free-spacing ratio
		t	Baffle thickness (m)
		T	Temperature ($^\circ C$)
		U	Average velocity ($m s^{-1}$)
		V	Volumetric flow rate ($m^3 s^{-1}$)
		V	Velocity ($m s^{-1}$)
		V	Voltage (V)
		w	Wetted parameter (m)

✉ S. Eiamsa-ard
smith@mut.ac.th

A. Phila
arnut_phila@hotmail.com

C. Thianpong
cthianpong@hotmail.com

¹ Faculty of Engineering, Mahanakorn University of Technology, Bangkok, Thailand

² Faculty of Engineering, King Mongkut's Institute of Technology Ladkrabang, Bangkok, Thailand



W	Channel width (m)
x	Local distance in the test section (m)
y/w	Twist ratio

Greek Symbols

ρ	Fluid density (kg m^{-3})
μ	Fluid dynamic viscosity ($\text{kg s}^{-1} \text{m}^{-1}$)
ν	Kinematic viscosity ($\text{m}^2 \text{s}^{-1}$)
η	Thermal enhancement factor
θ	Attack angle ($^\circ$)

Subscripts

abs	Absorbed heat
act	Actual heat
b	Bulk
c	Cross-section
e	Electrical
h	Hydraulic
i	Inlet
l	Loss
o	Outlet
w	Wall
x	Local distance of x -axis
0	Bare channel

Abbreviations

AR	Aspect ratio
PLA	Polylactic acid
RTD	Resistance temperature detector
TLC	Thermochromic liquid crystal

1 Introduction

Most manufacturing processes release waste heat in various forms—hot solid wastes, hot air or gases, or hot water, depending on the process. Waste heat can be recovered and further used. There are various devices and tools that enable waste heat reuse. Heat exchangers have been widely used for many years. Generally, a heat exchanger allows the transfer of heat from one liquid to another, where the liquids do not necessarily mix. This type of equipment is crucial in a wide variety of industries and engineering systems. For example, in the oil industry, heat exchangers are used to heat raw oil, condense vapor in a distillation tower into liquid, or decrease the temperature of an oil or gas. They are widely used in the food industry for the thermal treatment of foods to concentrate them or to assure public health.

As there are various uses for heat exchangers, selecting an optimal heat exchanger is complicated and an unsophisticated user generally would require professional assistance to select a suitable model. Heat exchanger software and manufacturers often evaluate heat exchangers according to various factors, although pricing and manufacturing costs play an

important role in decision making. Important factors that need to be considered include pressure limitations, thermal efficiency, temperature range, product composition, the pressure drop within the heat exchanger, required liquid flow rates, ease of cleaning, maintenance and repair, required materials of construction, future expansion, and materials of construction [1–3]. There are three common types of technique used to enhance the efficiency/performance of heat exchangers: (1) active methods, or techniques, that require external energy to aid in heat transfer (e.g., pulsation by cams [4], mechanical aids [5], surface and fluid vibration [6], suction or injection [7], and electrostatic fields [8]), (2) passive methods, or techniques, that modify the characteristics of the heat transfer channel (e.g., treated surfaces [9], rough surfaces [10], extended surfaces [11–13], swirl flow devices [14], and additives to fluids [15]), and (3) compound methods, or techniques, that combine both the active method and the passive method (e.g., rough surfaces with twisted tapes [16] and rough surfaces with fluid vibration [17]).

Passive methods have been applied extensively to improve heat transfer. Most studies examining them have dealt with the heat transfer characteristics of circular tubes, while rectangular channels have been scarcely reported. Changcharoen and Eiamsa-ard [18] investigated the flow pattern and heat transfer characteristics in a rectangular channel with a width-to-height aspect ratio of 6:1. The rectangular channel was equipped with detachable ribs placed on one side of the walls. The dependence of the Nusselt number on the Reynolds number was implicit, while an indirect association was observed for the friction factor. The ribs with a detached-clearance value (c/a) of 0.1 gave the maximum thermal efficiency at the lowest Reynolds number of 8000. Promvongse [19] found that incorporating multiple 60° V-baffle turbulators into a rectangular channel significantly improved heat transfer. Experiments were performed at various baffle pitch spacing ratios, (i.e., $PIH=1.0, 2.0,$ and 3.0) and baffle blockage ratios (i.e., $e/H=0.1, 0.2,$ and 0.3), while the transverse pitch remained unchanged at $2H$. The results showed that the Nusselt number increased with increasing Reynolds numbers. The optimal e/H and PIH ratios, where the maximum thermal enhancement factor ($\eta=1.87$) took place, were 0.1 and 1.0, respectively, at a minimum Reynolds number. The effect of the aspect ratio of a rectangular channel on both heat and mass transfer was studied by Lee et al. [20]. Their study was carried out in a rectangular channel, which had two types of V-shaped ribs placed inside—multiple-stagger ribs with a 45° attack angle and 60° continuous ribs. The results showed that the aspect ratio had a significant impact on both heat and mass transfer, and the impact was even more pronounced for the continuous 60° V-shaped rib. The effect of the multiple twisted tape vortex generators on thermal and flow characteristics in a turbulent flow channel was studied by Eiamsa-ard [21]. A rectangular channel with



a low free-spacing ratio (s/w) and a low twist ratio (y/w) has been proven successful in enhancing heat transfer. The pressure loss, however, has been found to increase.

A diversity of baffle geometrics (e.g., straight-shaped, V-shaped, and arc-shaped) and baffle arrangements, as shown in Fig. 1, has attracted a lot of attention in the heat transfer enhancement field for many years [1, 19–27]. To study the effects of the baffle on the local and average heat transfer coefficient and pressure drop, most of these studies have arranged the baffles perpendicular to the flow passage, i.e., placing the baffles straight up with respect to the x - y plane (the bottom surface of a channel), see Fig. 1a, b. The influences of the baffle angle orientation have been performed by varying the attach angle about the z -axis (pointing out of the paper), see Fig. 1c–f.

In contrast to previous works, in this study, the baffles were mounted on the x - z plane (on two side-walls of a channel), see Fig. 1h, so that we could orient them either in parallel ($\theta=0^\circ$ or 180°) or perpendicular ($\theta=90^\circ$) to the flow direction or even position them in-between (baffles are able to rotate about the y -axis). The study with most relevance

to this work was by Khan et al. [27], see Fig. 1g). However, they utilized only a single inclined baffle combined with periodic ribs, and they had only a marginal change in attack angles (3.5° – 7°), while our study used inclined baffles placed in series (continuous baffles) and allowed them to rotate with different attack angles from 0° to 180° . The differences in the numbers of baffles and attack angles will definitely result in dissimilar flow patterns and heat transfer rates. Furthermore, this current study distinguished itself by implementing the thermochromic liquid crystal (TLC) technique for surface temperature measurement without direct contact. This temperature measuring technique enabled us to determine the temperature of the entire heated surface, whereas it would likely have been very difficult for the conventional thermocouple method, as typically applied in the literature [20, 28], due to the constrained space and a need for numerous thermocouples [19, 23–27]. It is also important to note that by analyzing image processing the detailed temperature contours of the heated surface can be produced effectively. This study was aimed at evaluating the impacts of the attack angle of inclined baffles incorporated

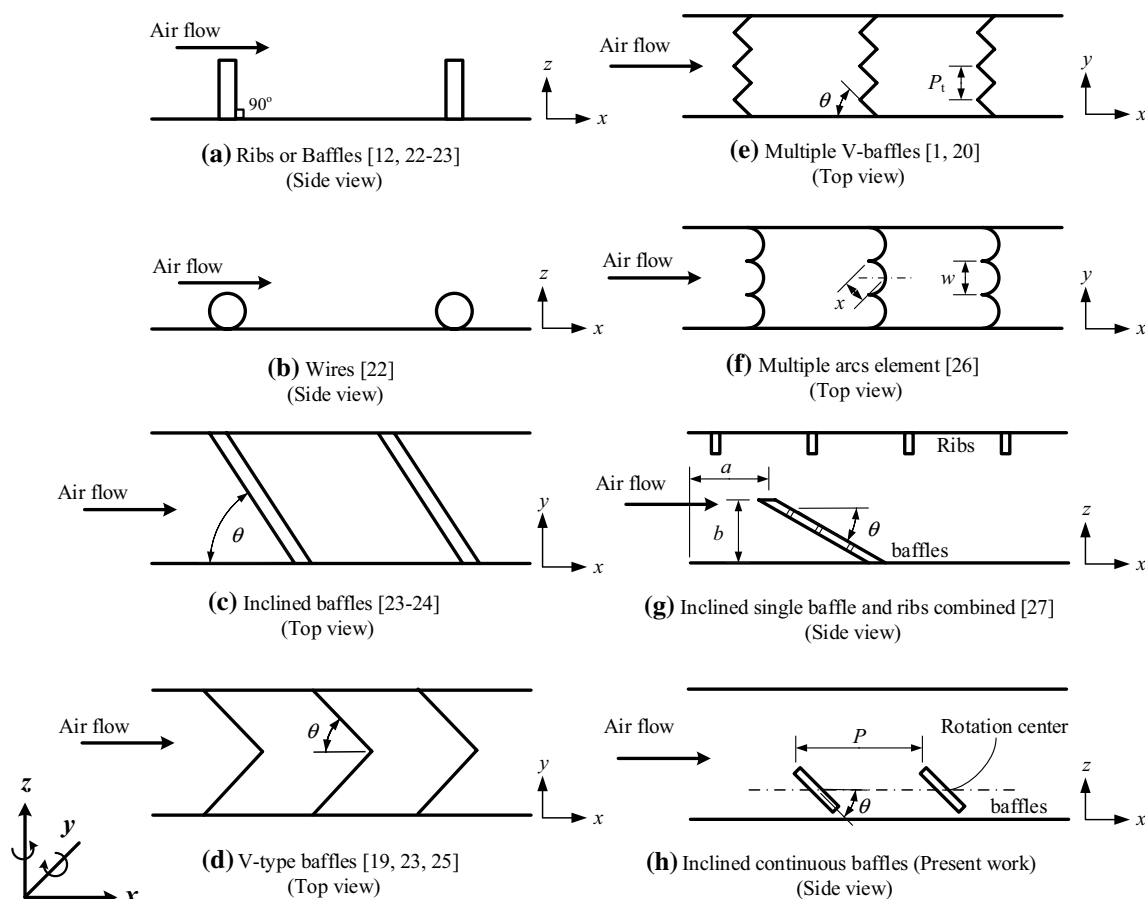


Fig. 1 Configurations of eight different primary shapes: **a** rectangular ribs, **b** wires, **c** inclined baffles, **d** V-type baffles, **e** multiple V-baffles, **f** inclined single baffle and ribs, and **g** inclined continuous baffles

into a rectangular channel on heat transfer and pressure loss characteristics. Unlike previous studies, the baffles were differentiated by their configuration and capability to regulate any inclination from horizontal ($\theta=0^\circ, 180^\circ$) and vertical ($\theta=90^\circ$). Instead of a conventional thermocouple technique, the TLC image processing technique was utilized to clarify the temperature distributions on the heated surface. The resulting Nusselt numbers, frictional factors, and thermal enhancement factors were examined for the Reynolds number ranging from 9000 to 24,000. For comparison, experiments for a bare channel were also performed.

2 Experimental Setup

2.1 Thermochromic Liquid Crystal

Being manageable, economical, reliable, and almost noninvasive, the thermochromic liquid crystal (TLC) technique is becoming an increasingly interesting technique for measuring the surface temperature. It is highly sensitive and responsive to temperature by changing its color against the modified temperature. To measure the surface temperature, either direct placement of TLCs on a surface or suspension in the fluid is possible. The uniform, steady-state surface temperature method proposed by Abdullah et al. [29] and Grassi et al. [30] was applied for calibrating the TLCs in this study. The calibrated surface was heated to a selective temperature range of TLCs, while the color was quantified by a digital camera. An image processing program enabled us to interpret the color of each of the obtained entire color images for a known temperature and convert them to either a fraction of the individual three primary colors—red (R), green (G), and blue (B)—or RGB coordinates. Although all colors were a weighted combination of three primary colors, it was more convenient to associate them with another three characteristics—hue, saturation, and value (HSV coordinates). However, only hue (H) representing the spectral colors could transform these primary colors to the corresponding temperature. A relationship of H and RGB can be mathematically formulated as shown in Eq. 1 [30]:

$$H = \frac{\cos^{-1} \left[\frac{R - \frac{G+B}{2}}{\sqrt{(R-G)^2 + (R-B)(G-B)}} \right]}{2\pi}, \quad H, R, G, B \in [0.1] \quad (1)$$

Figure 2 shows the temperature varying with the H value. By least-squares fitting with a third order polynomial, a T – H correlation is available as follows:

$$T_w = 0.000262 H^3 - 0.112715 H^2 + 16.167973 H - 744.041481 \quad (2)$$

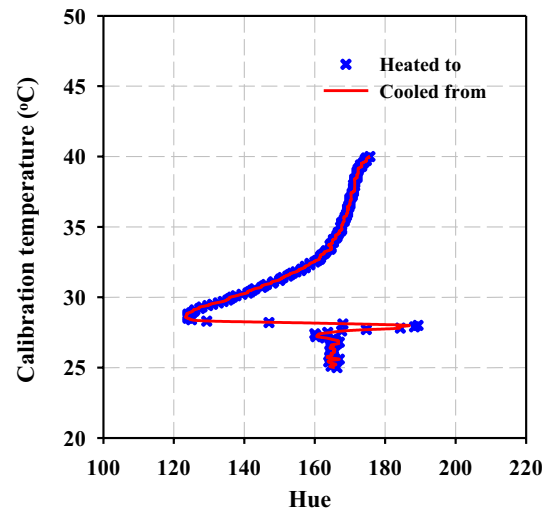


Fig. 2 Hue–temperature calibrations of TLC sheets (TLCs were heated or cooled)

Table 1 Dimensionless quantities and other parameters used in test section experiments

<i>Test section</i>	
Channel height, H (mm)	40
Channel width, W (mm)	150
Channel length, L (mm)	900
Aspect ratio, AR	3.75
<i>Inclined baffle</i>	
Material	PLA plastic
Thickness of baffle, t (mm)	1.0
Height of baffle, e (mm)	6.0 ($e/H=0.15$)
Width of baffle, l (mm)	150
Pitch length, P (mm)	60 ($P/e=10$)
Attack angles, θ ($^\circ$)	0° (or 180°), 15° , 30° , 45° , 60° , 75° , 90° , 105° , 120° , 135° , 150° and 165°
<i>Test conditions</i>	
Working fluid	Air
Reynolds number, Re	9000–24,000
Prandtl number, Pr	0.7

2.2 Roughness Geometry and Range of Parameters

Table 1 contains the experimental design and operating conditions. The roughness parameters associated with the inclined baffles were characterized by the baffle height (e), pitch length (P), and channel height (H). The pitch length to baffle height ratio (P/e) in this study was equal to 10, based on the optimum value reported in previous work [20, 22]. The baffle height to channel height ratio (e/H) was set to be 0.15 for efficient heat transfer [20, 31]. Figure 3 shows the arrangement of inclined baffles (side view) placed inside the

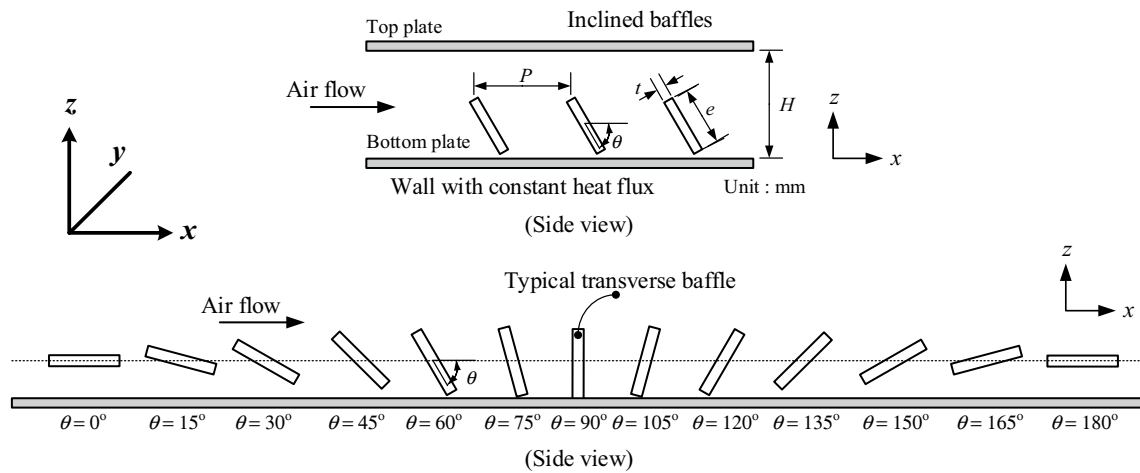


Fig. 3 Geometry of rectangular channel flow with inclined baffles at various attack angles

rectangular channel. The baffles could freely rotate in a vertical plane about the y -axis (pointing out of the paper), allowing the attack angle to be varied from horizontal ($\theta = 0^\circ$, 180°) to vertical ($\theta = 90^\circ$) with a 15 degrees instrument. The configuration of the baffle was designed by a special engineering program (solidworks). The baffles, made of polylactic acid (PLA) plastic, were molded by a 3D plastic printer.

2.3 Experiment Apparatus and Procedure

The experimental apparatus, schematically shown in Fig. 4, consisted of three parts—rectangular channel, image processing, and analysis and computerized data acquisition sections. A rectangular channel was made of 10 mm thick acrylic with 40 mm (width) \times 150 mm

(height) \times 3500 mm (length). The channel contained inlet, test, and outlet sections with lengths of 2000 mm, 900 mm, and 600 mm, respectively. The unheated inlet section had a length of 2000 mm, which was quantified from the correlation developed by Ower and Pankhurst [32], to ensure the fully developed turbulent flow before entering the heated test section. The test section bottom wall was electrically heated under a constant heat flux condition by the controlled heating elements. The electrical power supplied was held constant at 60 W throughout the test period. The entire heated test section was well insulated to minimize heat loss. Air flow was supplied through a high-pressure blower equipped with a frequency inverter and measured by a well-calibrated orifice plate.

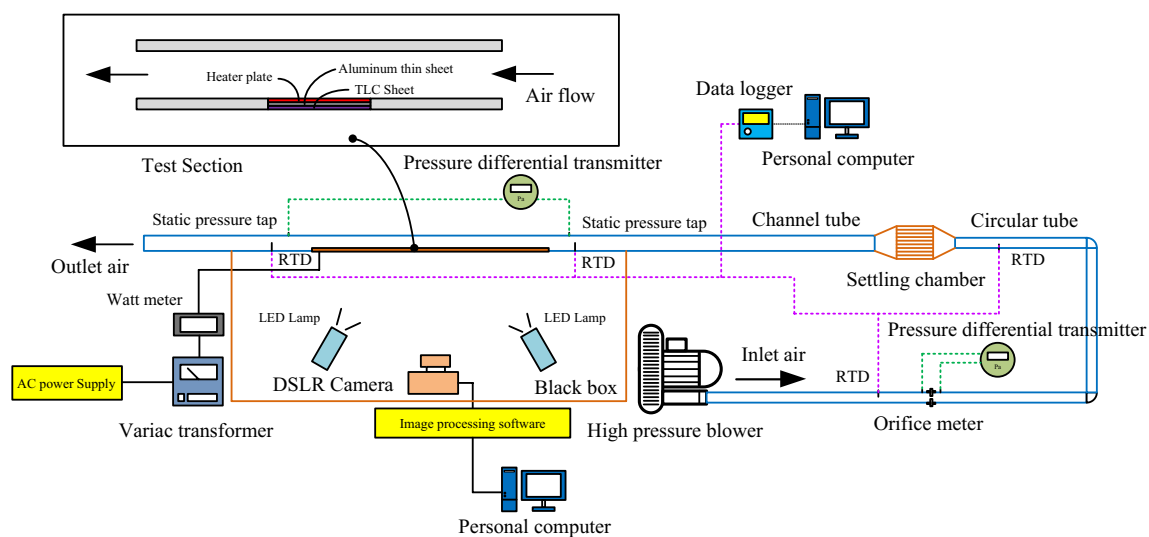


Fig. 4 Schematic diagram of experimental apparatus

Three resistant temperature detectors (RTDs) were mounted at the test section inlet and another eight were mounted at the outlet for measuring the inlet and outlet air temperature. Pressure drop, used to determine the friction factor, was determined by a digital differential transmitter. Both temperature and pressure drop were continuously monitored via a computerized data acquisition system. The bottom surface of the heated test surface section was instrumented with TLCs to quantify the temperature distribution on the heated surface. The TLCs used in this study were manufactured by Omega Engineering Co., Ltd., and they were designed to operate in a temperature range of 30–35 °C. The clear acrylic walls of the test section were visible to a digital camera which communicated with a computer. The obtained images were then analyzed by an image processing program.

The uncertainties of average velocity (U), volumetric air flow rate (V), static pressure (P), and temperature (T), which were estimated based on ANSI/ASME [33], were found to be within $\pm 5.2\%$, $\pm 4.7\%$, $\pm 4.2\%$, and $\pm 0.5\%$, respectively. The uncertainty of the non-dimensional parameters of Reynolds number, Nusselt number, and friction factor were within $\pm 4.6\%$, $\pm 7.5\%$, and $\pm 5.9\%$, respectively.

Prior to running the experiments, all measuring devices were carefully calibrated and the system was checked for leakage. The experiments were performed at a constant heat flux. All experimental data were taken under steady-state conditions that had remained stable for over 60 min. The recorded data are listed as follows:

- (i) Temperature of the surface of the test channel;
- (ii) Inlet and outlet temperatures of air;
- (iii) Pressure drop across the test section;
- (iv) Voltage and current through the electrical heating plate.

3 Theoretical Aspects

The recorded data were used to evaluate the heat transfer coefficient (h), friction factor (f), and the thermal enhancement factor (η).

The Reynolds number, based on the hydraulic diameter of the test section, was evaluated from [34]:

$$Re = \frac{V_i D_h}{\nu} \quad (3)$$

where V_i is the inlet air velocity, D_h is the hydraulic diameter of test channel, and ν is the kinematic viscosity of air.

The mass flow rate was calculated by [34]:

$$\dot{m} = \rho V_i A_c \quad (4)$$

where ρ is the bulk density of air at a specific temperature and A_c is the cross-sectional area of a rectangular channel.

The total heat supplied by the electric heating plate was calculated as

$$Q_e = VI \quad (5)$$

where V and I are the supplied voltage and current to the electric heating plate, respectively.

The actual heat supplied to the test equipment by the electrical heating plate (Q_{act}) was

$$Q_{act} = Q_e - Q_l \quad (6)$$

The heat loss (Q_l) through the insulation evaluated from the average wall temperatures and the ambient air temperatures was approximately 1–3% of the total heat supplied from the heat source.

The heat transferred to air flow was evaluated by [35]

$$Q_{abs} = \dot{m} C (T_o - T_i) \quad (7)$$

where \dot{m} is the mass flow rate, C is the specific heat capacity of air, and T_i and T_o are the inlet and outlet air temperatures, respectively.

The difference between the heat supplied (Q_{act}) and the heat absorbed by the fluid (Q_{abs}) was less than 5% in all experiments. The heat transfer rate (Q) was estimated as the mean value of the actual heat supplied by the electric heating plate and the heat absorbed by the fluid as

$$Q = \frac{Q_{act} + Q_{abs}}{2} \quad (8)$$

Heat flux can be expressed as

$$q = \frac{Q}{WL} \quad (9)$$

where W and L are the width and length, respectively, of the electric heating plate.

The local convective heat transfer coefficient can be estimated from

$$h_x = \frac{q}{(T_{wx} - T_{bx})} \quad (10)$$

where T_{bx} and T_{wx} are the local bulk air and thermochromic liquid crystal surface temperatures, respectively.

The local bulk air temperatures were calculated by an energy balance:

$$T_{bx} = T_i + \frac{q(wx)}{\dot{m}C} \quad (11)$$

where w is the wetted perimeter and x is the local distance of the test section.

The local Nusselt number can be expressed as

$$Nu_x = \frac{h_x D_h}{k} \quad (12)$$

where k is the thermal conductivity of air.

The average local Nusselt number along the z -axis at any x -axis was called spanwise Nusselt number.

The average heat transfer coefficient was calculated from [35]

$$h = \frac{q}{(T_w - T_b)} \tag{13}$$

where T_b and T_w are the mean bulk air and thermochromic liquid crystal surface temperatures, respectively.

The average Nusselt number can be evaluated using the relationship [35]

$$Nu = \frac{hD_h}{k} \tag{14}$$

The friction factor was evaluated for a measured pressure drop from Darcy’s formula [34]:

$$f = \frac{\Delta P}{\left(\frac{L}{D_h}\right)\left(\rho_b \frac{V^2}{2}\right)} \tag{15}$$

where ΔP is the pressure drop across the test section.

The thermal enhancement factor (η) is defined as the ratio of the heat transfer coefficient of the channel with inclined baffles (h) to that of the channel with no baffles (h_0). The thermal enhancement factor under a constant pumping power criterion is

$$\eta = \frac{h}{h_0} = \left(\frac{Nu}{Nu_0}\right)\left(\frac{f}{f_0}\right)^{-1/3} \tag{16}$$

where Nu and f are the Nusselt number and friction factor of the channel with inclined baffles, respectively. Nu_0 and f_0 are the Nusselt number and friction factor of the bare channel with no baffles, respectively.

4 Experimental Results

4.1 Channel Without Baffles

To validate the experimental measurements, preliminary experiments were performed in a bare channel without any baffles. The resulting Nusselt number and friction factor were then compared to those calculated from Dittus–Boelter and Blasius correlations [35], respectively.

The Dittus–Boelter correlation (Eq. 17) is valid for $Re > 7000$ and $0.5 < Pr < 120$:

$$Nu = 0.023Re^{0.8}Pr^n \tag{17}$$

where $n=0.4$ for heating and $n=0.3$ for cooling.

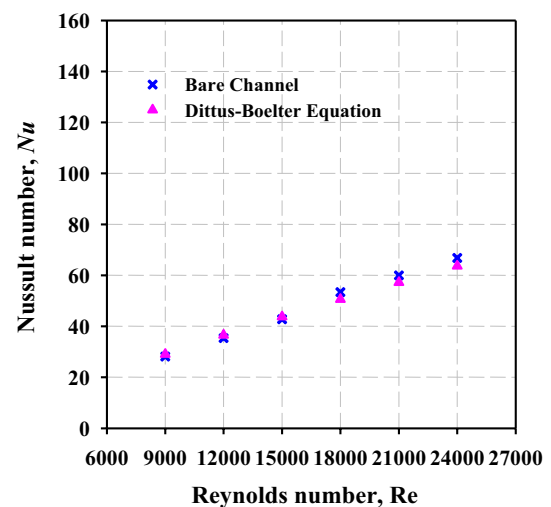


Fig. 5 Comparison of experimental and estimated values of the Nusselt number for a bare channel

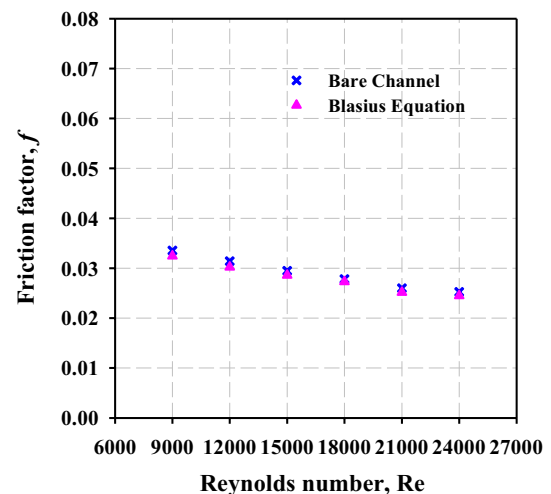


Fig. 6 Comparison of experimental and estimated values of friction factor for a bare channel

The present work involved heating, therefore, the correlation can be re-written as

$$Nu = 0.023Re^{0.8}Pr^{0.4} \tag{18}$$

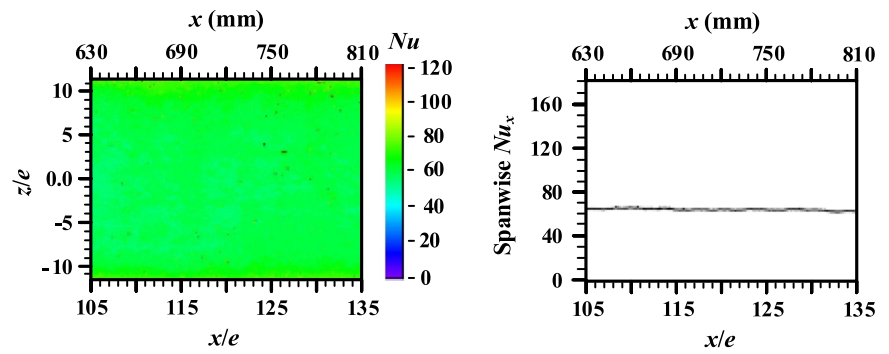
The Blasius’s correlations are

$$f = 0.085Re^{-0.25} \quad \text{for } Re < 20,000 \text{ and} \tag{19}$$

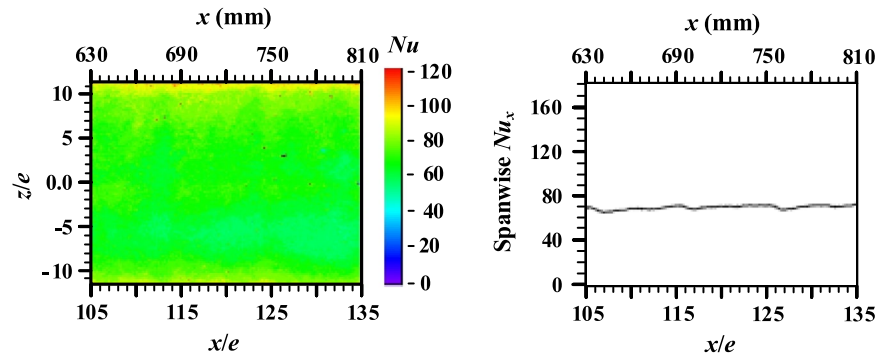
$$f = 0.184Re^{-0.2} \quad \text{for } Re \geq 20,000. \tag{20}$$

Figures 5 and 6 show a validation of our measurements through a good agreement between the Nusselt number and the friction factor experimented in a bare rectangular channel and those calculated from the well-known correlation

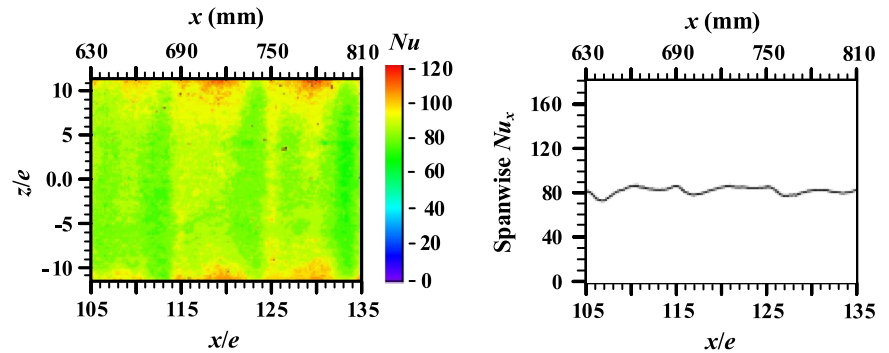
Fig. 7 Nusselt number field and spanwise Nusselt number of a channel with inclined baffles at a Reynolds number of 24,000: **a** bare channel and attack angles of **b** 0° , **c** 30° , **d** 60° , **e** 90° , **f** 120° and **g** 150°



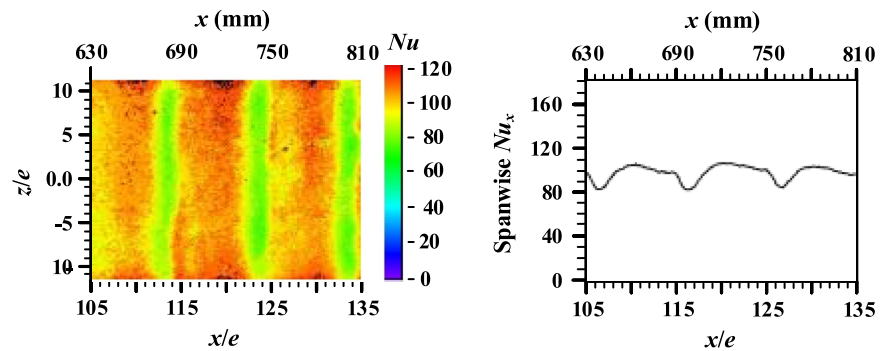
(a) Bare channel



(b) Inclined baffle ($\theta = 0^\circ$)

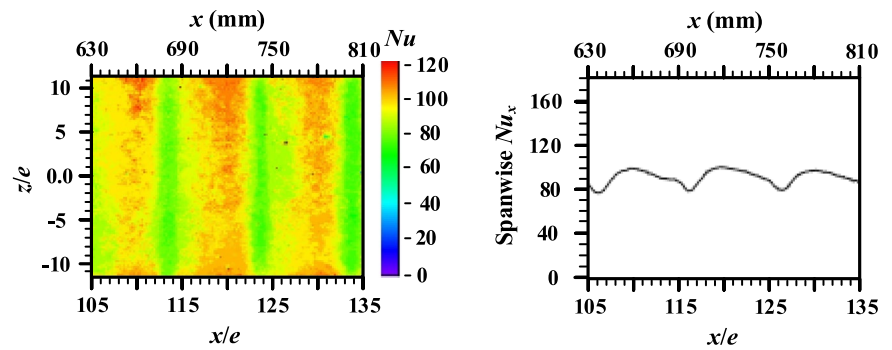


(c) Inclined baffle ($\theta = 30^\circ$)

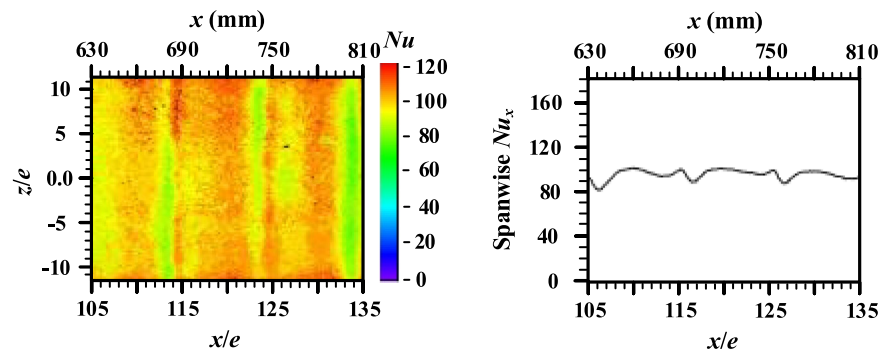


(d) Inclined baffle ($\theta = 60^\circ$)

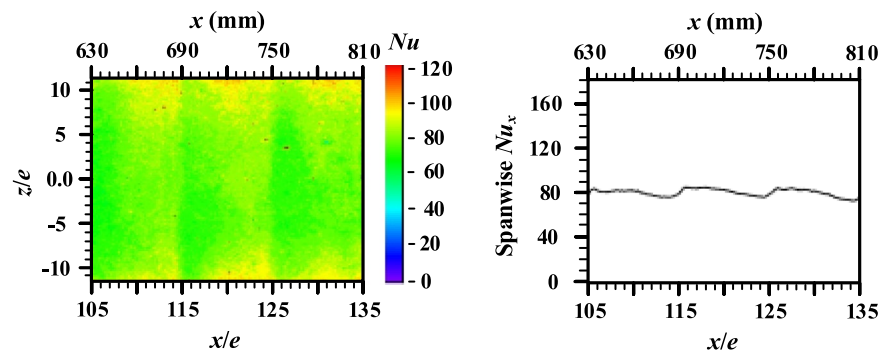
Fig. 7 (continued)



(e) Inclined baffle ($\theta = 90^\circ$)



(f) Inclined baffle ($\theta = 120^\circ$)



(g) Inclined baffle ($\theta = 150^\circ$)

(Eqs. 18, 19, and 20). The experimental results deviated from the correlation by $\pm 6\%$ for the Nusselt number and $\pm 4\%$ for the friction factor.

4.2 Distribution and Spanwise Nusselt Number

Nusselt number distributions over the heated bottom wall of a rectangular channel with inclined baffles at various attack angles (from 0° to 165°) are depicted in Fig. 7. The experiments for a rectangular channel with no baffles were also performed, and the results are shown in the same figure for comparison. The Reynolds number was held constant at 24,000 for all the results shown in the figure. Implicitly,

the intermediate attack angles (45° – 135°) were efficient in promoting a high local Nusselt number (in the x -direction) compared to the low and high attack angles (i.e. 0° – 30° and 150° – 165° , respectively). It is possible that the intermediate attack angles contributed a greater turbulence due to a high degree of blockage. This is in accordance with the results depicted in Fig. 8 showing that a strong flow disturbance and fluctuation took place at this angle range. Moreover, such a flow could effectively disturb the thermal boundary layer making it thinner, thereby reducing the resistance to heat transfer. As a result, the Nusselt number was greater. The maximum heat transfer coefficient enhanced by the turbulent flow in the vicinity of the reattachment point behind the

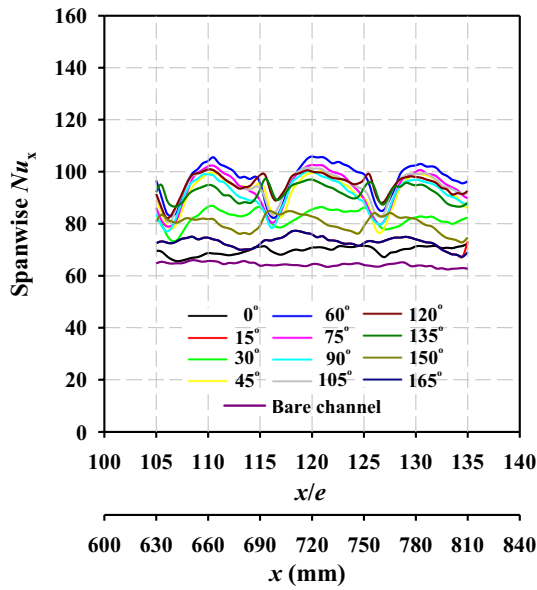


Fig. 8 Distribution of local Nusselt number in the rectangular channel with inclined baffles at various attack angles

baffles was also reported by Changcharoen et al. [18], Prasad et al. [22], and Karwa [23]. Such findings agree closely to the numerical results reported by Boonloi and Jedsadaratanachai [1] and Yongsiri et al. [24]. Alternatively, the flow across the baffles with low attack angles could have been subjected to a weaker disturbance.

4.3 Heat Transfer and Pressure Loss

The variation of the Nusselt number with the attack angle and with the Reynolds number are presented in Fig. 9a, b, respectively, to show the impact of inclined baffles on heat transfer. Additionally, to represent the improved heat transfer, the relative Nusselt number, defined as the ratio of the Nusselt number of a baffle integrated channel to the Nusselt number of a bare channel (Nu/Nu_0), was plotted against the Reynolds number (Fig. 9c). In Fig. 9a, at a given Reynolds number, the Nusselt number associated with the intermediate range of the attack angle (45° – 135°) was higher than those obtained from the two extreme conditions (i.e., 0° – 30° and 150° – 165°). Among the intermediate angles, the 60° and 120° angles yielded the highest Nusselt numbers. In Fig. 9b, the Nusselt number tended to increase with the Reynolds number. This was due to the intensified flow turbulence and consistent with results found elsewhere [18–20, 23, 36]. Although a direct relationship between the Nusselt and the Reynolds numbers is clear for all the attack angles (as shown in Fig. 9b), an inverse relationship between the relative Nusselt number (representative of improved heat transfer) and the Reynolds number can be seen in Fig. 9c. The maximum improvement in heat transfer at particular

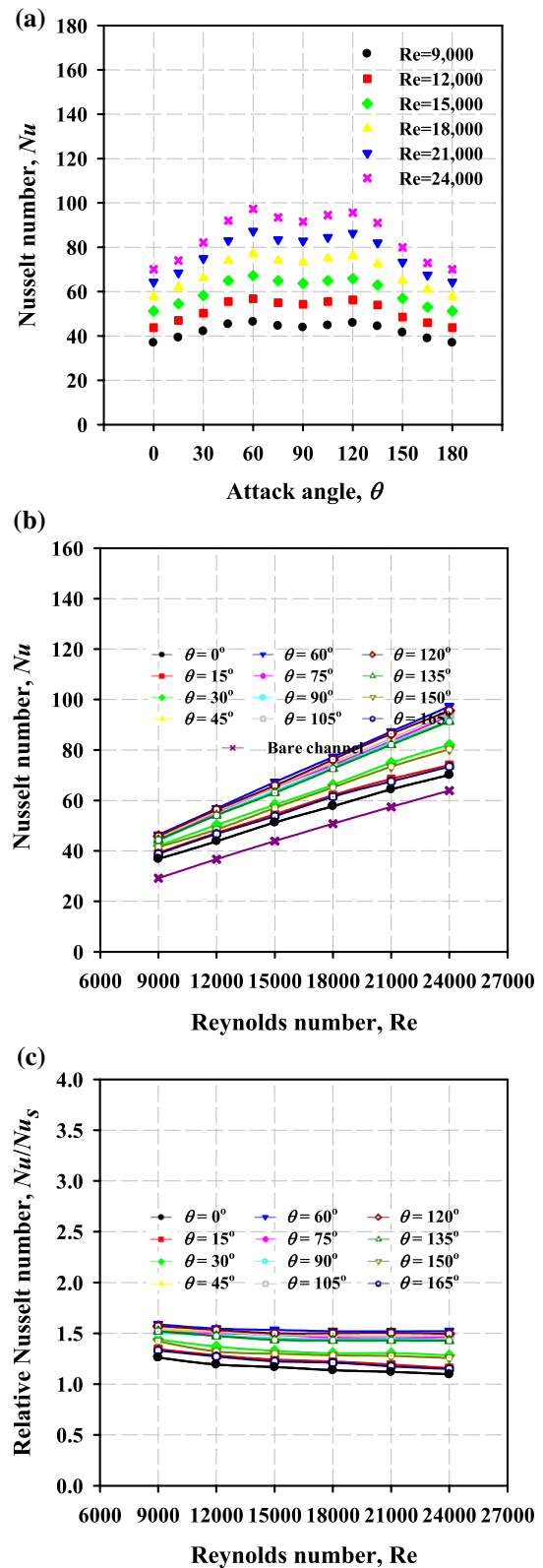


Fig. 9 Effect of attack angle of inclined baffles on the Nusselt number: **a** Nu versus θ , **b** Nu versus Re , and **c** Nu/Nu_0 versus Re

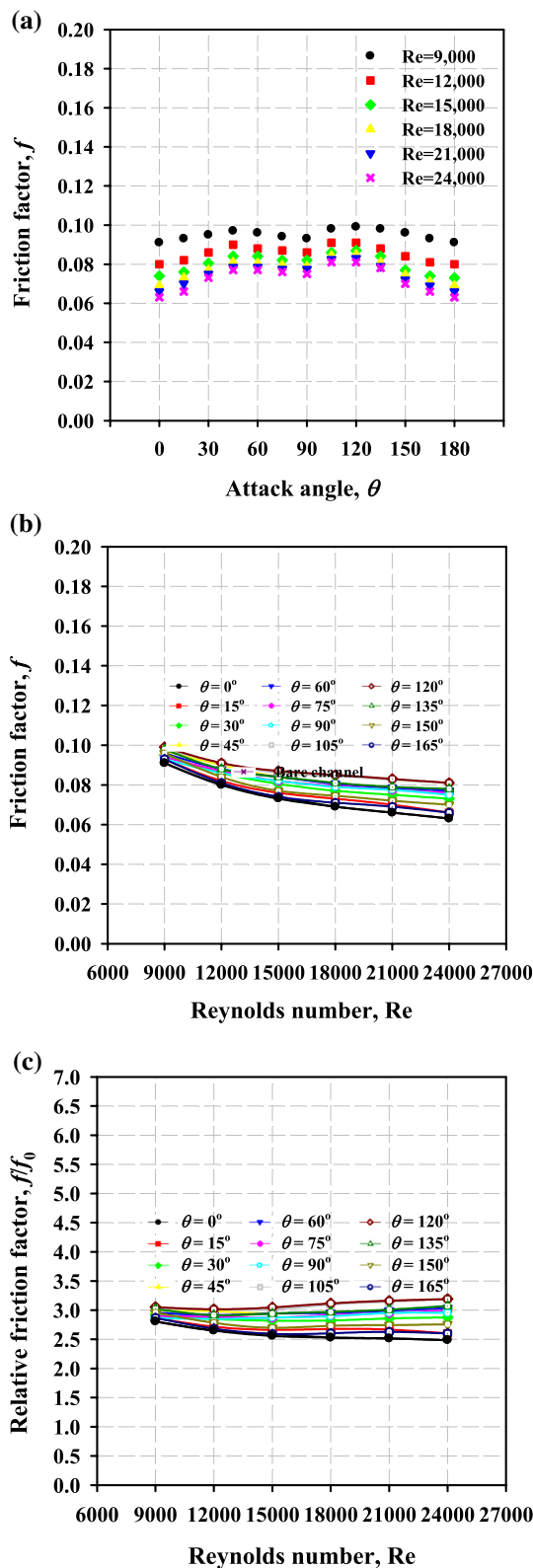


Fig. 10 Effect of attack angle of inclined baffles on the friction factor: **a** f versus θ , **b** f versus Re , and **c** f/f_0 versus Re

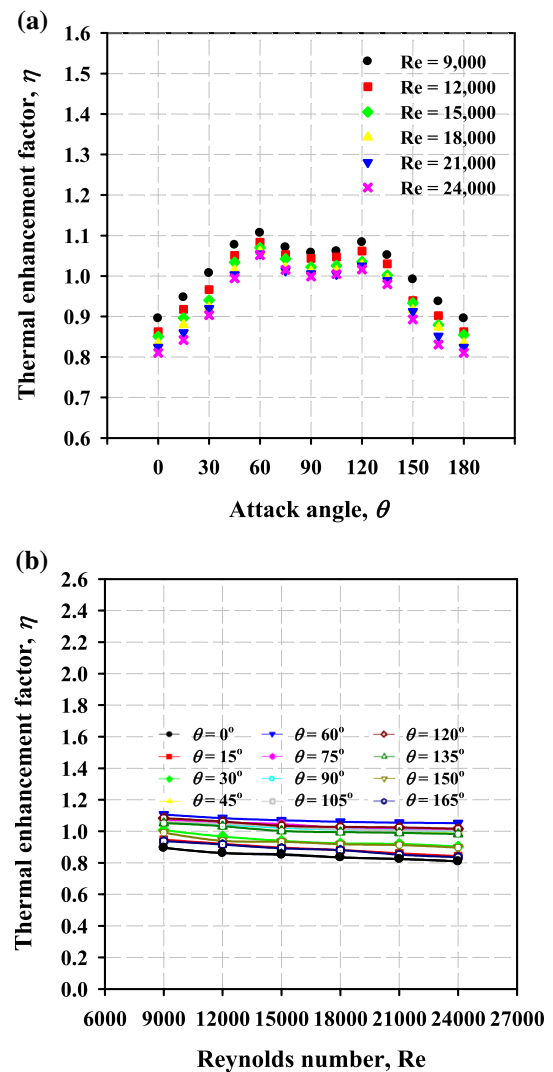


Fig. 11 Effect of attack angle of inclined baffles on the thermal enhancement factor: **a** η versus θ and **b** η versus Re

attack angles coincided with a Reynolds number of 9000 and ranged between 1.26 and 1.59 times of the bare channel. The most efficient heat transfer enhancement was achieved at attack angles of 60° and 120° with the respective relative Nusselt numbers of 1.59 and 1.57 times of the bare channel.

To explore the effect of the inclined baffles on the pressure drop in a rectangular channel, the friction factor (f) and relative friction factor (f/f_0) were plotted against the attack angle (θ) and the Reynolds number (Re), as shown in Fig. 10a–c. As discussed above, a greater air flow blockage accompanied by high turbulence for intermediate attack angles (45° – 135°) enhanced heat transfer, with a concurrent adverse effect on the frictional losses, as shown in Fig. 10a. As expected, the friction factor continued to decline as the Reynolds number increased, as is shown in Fig. 10b. A common agreement has also been addressed in the literature [10, 13, 14, 21, 23]. This contributed to an increased

Table 2 Comparison of different roughnesses

Researchers	Roughness	Parameter	η
Changcharoen et al. [18]	Detached rib	$c/a=0.1-0.4$, $WH=6$, $P/e=10$, $Re=4000-16,000$	1.22
Promvonge et al. [38]	Combined rib and delta winglet	$\alpha=30^\circ-90^\circ$, $Re=5000-22,000$	1.39
Karwa et al. [39]	Chamfered rib	$P/e=4.53-8.54$, $WH=4.65-12.0$, $\varphi=-15^\circ$ to 15° , $Re=2000-20,000$	1.39
Promvonge et al. [40]	Rectangular rib	$P/e=6.67$, $e/H=0.3$, $Re=4000-16,000$	0.91
Promvonge et al. [40]	Triangular rib	$P/e=6.67$, $e/H=0.3$, $Re=4000-16,000$	1.04
Present study	Inclined baffle	$P/e=10$, $e/H=0.15$, $\theta=0^\circ-180^\circ$, $Re=9000-24,000$	1.11

flow turbulence. The impact of the inclined baffles on the pressure drop over that of a bare channel is also seen in Fig. 10c. All the relative friction factors (ff/f_0) were in the range of 2.48–3.19, much greater than unity even for $\theta=0^\circ$. At the minimum Reynolds number, 9000, each intermediate attack angle had a slightly different friction factor. This may have been due to the lower turbulence associated with these smaller Reynolds numbers not being high enough to significantly affect the pressure drop at these angles. For comparisons with similar Reynolds numbers, the obtained friction factors in this work (2.48–3.19) were lower than those obtained from the transverse rib (2.68–2.94), inclined rib (3.02–3.42), V-up continuous rib (3.40–3.93), and V-down continuous rib (3.32–3.65), as reported by [23]. The present inclined baffle, however, showed results superior to the V-up discrete rib (2.35–2.47) [23] and the V-down discrete rib (1.96–2.58) [23, 37].

4.4 Thermal Enhancement Factor

To investigate the synergetic effect of the attack angle on heat transfer and friction loss, the thermal enhancement factor (η), defined in Eq. (16), was plotted against the attack angle, as shown in Fig. 11a. Only at the intermediate attack angles ($45-135^\circ$) was the thermal enhancement factor greater than unity. At these angles, there was more gain from heat transfer than loss from friction. The thermal enhancement factor reached its zenith (about 1.11) at the attack angles of 60° and 120° and at a Reynolds number of 9000. Figure 11b reveals that the thermal enhancement

factor tended to decrease a little as the Reynolds number moved further from 9000.

Table 2 summarizes the maximum thermal enhancement factors reported in the relevant studies and the one obtained from the present study for comparisons. The current inclined baffle was more effective than the rectangular rib by 22% and the triangular rib by 7%. However, it was likely to be inferior to others by 10–25%, depending on the rib type.

5 Conclusions

The following conclusions can be drawn from the results of this study:

1. Introducing inclined baffles into a rectangular channel resulted in the fluctuation of the Nusselt number, as reflected by the local Nusselt number distribution in the direction of flow over the heated bottom of the channel. The fluctuations were more noticeable at the intermediate attack angles ($45^\circ-135^\circ$) than at the lower and higher angles ($0^\circ-30^\circ$ and $150^\circ-165^\circ$, respectively);
2. As a consequence of high blockage and turbulence, the baffles at the intermediate attack angles produced a higher pressure drop, but a markedly increased heat transfer;
3. Among the intermediate attack angles, 60° yielded the highest heat transfer rate, which was 1.59 times as much as that obtained from a bare rectangular channel;
4. Only the intermediate attack angles produced thermal enhancement factors greater than unity. The thermal enhancement factor represents the combined effects of heat transfer and frictional loss, implying the thermal advantage of using these inclined baffles although a larger pressure drop occurred. The maximum thermal enhancement factor of 1.11 took place when $\theta=60^\circ$ and at a Reynolds number of 9000;
5. The TLC technique employed in this work has been proven powerful and effective for quantifying the temperature distribution of the heated surface.

References

1. Boonloi, A.; Jedsadaratanachai, W.: Turbulent forced convection in a heat exchanger square channel with wavy-ribs vortex generator. *Chin. J. Chem. Eng.* **23**, 1256–1265 (2015)
2. Jain, P.K.; Lanjewar, A.: Overview of V-RIB geometries in solar air heater and performance evaluation of a new V-RIB geometry. *Renew. Energy* **133**, 77–90 (2019)

3. Yang, W.; Xue, S.; He, Y.; Li, W.: Experimental study on the heat transfer characteristics of high blockage ribs channel. *Exp. Therm. Fluid Sci.* **83**, 248–259 (2017)
4. Sivakumar, K.; Natarajan, E.; Kulasekharan, N.: Influence of rib height on heat transfer augmentation: application to aircraft turbines. *Int. J. Turbo Jet Engines* **31**, 87–95 (2014)
5. Seghir-Ouali, S.; Saury, D.; Harmand, S.; Phillipart, O.; Laloy, D.: Convective heat transfer inside a rotating cylinder with an axial air flow. *Int. J. Therm. Sci.* **45**, 1166–1178 (2006)
6. Veerapandi, R.; Karthikeyanb, G.; Jinuc, G.R.; Kannaiah, R.: Experimental study and analysis of flow induced vibration in a pipeline. *Int. J. Eng. Res. Technol.* **3**, 1996–1999 (2014)
7. Attia, H.A.: Unsteady MHD couette flow with heat transfer in the presence of uniform suction and injection. *Mech. Mech. Eng.* **12**, 165–176 (2008)
8. Gorla, R.S.R.; Gatica, J.E.; Ghorashi, B.; In-Eure, P.; Byrd, L.W.: Heat transfer in a thin liquid film in the presence of electric field for non-isothermal interfacial condition. *Int. J. Fluid Mech. Res.* **29**, 146–157 (2002)
9. Kim, H.Y.; Kang, B.H.: Effects of hydrophilic surface treatment on evaporation heat transfer at the outside wall of horizontal tubes. *Appl. Therm. Eng.* **23**, 449–458 (2003)
10. Pawar, C.B.; Aharwal, K.R.; Chaube, A.: Heat transfer and fluid flow characteristics of rib-groove roughened solar air heater ducts. *Indian J. Sci. Technol.* **2**, 50–54 (2009)
11. Hasan, A.; Siren, K.: Performance investigation of plain and finned tube evaporatively cooled heat exchangers. *Appl. Therm. Eng.* **23**(3), 325–340 (2003)
12. Eiamsa-ard, S.; Promvong, P.: Thermal characteristics of turbulent rib-grooved channel flows. *Int. Commun. Heat Mass Transf.* **36**, 705–711 (2009)
13. Kanna, P.R.; Sivasubramanian, M.; Prabu, P.M.; Uthayakumar, M.: Numerical simulation of steady flow and forced convection heat transfer from two square cylinders placed in a channel. *Arab. J. Sci. Eng.* **42**, 1795–1815 (2017)
14. Eiamsa-ard, S.; Promvong, P.: Enhancement of heat transfer in a circular wavy-surfaced tube with a helical-tape insert. *Int. Energy J.* **8**, 29–36 (2007)
15. Eiamsa-ard, S.; Kiatkittipong, K.: Heat transfer enhancement by multiple twisted tape inserts and TiO_2 /water nanofluid. *Appl. Therm. Eng.* **70**, 896–924 (2014)
16. Patil, S.D.; Patil, A.M.; Kamble, G.S.: Analysis of twisted tape with straight winglets to improve the thermo-hydraulic performance of tube in tube heat exchanger. *Int. J. Adv. Eng. Res. Stud.* **1**, 99–103 (2012)
17. Alamgholilou, A.; Esmaeilzadeh, E.: Experimental investigation on hydrodynamics and heat transfer of fluid flow into channel for cooling of rectangular ribs by passive and EHD active enhancement methods. *Exp. Therm. Fluid Sci.* **38**, 61–73 (2012)
18. Changcharoen, W.; Eiamsa-ard, S.: Numerical investigation of turbulent heat transfer in channels with detached rib-arrays. *Heat Transf. Asian Res.* **40**, 431–447 (2011)
19. Promvong, P.: Heat transfer and pressure drop in a channel with multiple 60° V-baffles. *Int. Commun. Heat Mass Transf.* **37**, 835–840 (2010)
20. Lee, D.H.; Rhee, D.H.; Kim, K.M.; Cho, H.H.; Moon, H.K.: Detailed measurement of heat/mass transfer with continuous and multiple V-shaped ribs in rectangular channel. *Energy* **34**, 1770–1778 (2009)
21. Eiamsa-ard, S.: Study on thermal and fluid flow characteristics in turbulent channel flows with multiple twisted tape vortex generators. *Int. Commun. Heat Mass Transf.* **31**, 644–651 (2010)
22. Prasad, B.N.; Saini, J.S.: Effect of artificial roughness on heat transfer and friction in a solar air heater. *Sol. Energy* **41**, 555–560 (1988)
23. Karwa, R.: Experimental studies of augmented heat transfer and friction in asymmetrically heated rectangular ducts with ribs on the heated wall in transverse, inclined, V-continuous, V-discrete pattern. *Int. Commun. Heat Mass Transf.* **30**, 241–250 (2003)
24. Aharwal, K.R.; Gandhi, B.K.; Saini, J.S.: Experimental investigation on heat transfer enhancement due to a gap in an inclined continuous rib arrangement in a rectangular duct of solar air heater. *Renew. Energy* **33**, 585–596 (2008)
25. Momin, A.M.E.; Saini, J.S.; Solanki, S.C.: Heat transfer and friction in solar air heater duct with V-shaped rib roughness on absorber plate. *Int. J. Heat Mass Transf.* **45**, 3383–3396 (2002)
26. Pandey, N.K.; Bajpai, V.K.: Varun: heat transfer and friction factor study of a solar air heater having multiple arcs with gap-shaped roughness element on absorber plate. *Arab. J. Sci. Eng.* **41**, 4517–4530 (2016)
27. Khan, J.A.; Hinton, J.; Baxter, S.C.: Enhancement of heat transfer with inclined baffles and ribs combined. *Enhanc. Heat Transf.* **9**, 137–151 (2002)
28. Mehta, B.; Khandekar, S.: Measurement of local heat transfer coefficient during gas liquid Taylor bubble train flow by infra-red thermography. *Int. J. Heat Mass Flow* **45**, 41–52 (2014)
29. Abdullah, N.; Talib, A.R.T.; Jaafar, A.A.; Salleh, M.A.M.; Chong, W.T.: The basics and issues of thermochromic liquid crystal calibrations. *Exp. Therm. Fluid Sci.* **34**, 1089–1121 (2010)
30. Grassi, W.; Testi, D.; Vista, D.D.; Torelli, G.: Calibration of a sheet of thermo-sensitive liquid crystals viewed non-orthogonally. *Measurement* **40**, 898–903 (2007)
31. Agrawal, S.; Bhagoria, J.L.; Malviya, R.K.: A detailed review on artificial roughness geometries for optimizing thermo-hydraulic performance of solar air heater. *Int. J. Mod. Eng. Res.* **4**, 106–122 (2014)
32. Ower, E.; Pankhurst, R.C.: *Measurement of Air Flow*, 5th edn. Pergamon Press, Oxford (1977). (in SI units ed.)
33. ANSI/ASME, Measurement uncertainty, PTC 19, Part I, 1986; 1-1985
34. Kreith, F.; Berger, S.A.: *Mechanical Engineering Handbook*. CRC Press, Boca Raton (1999)
35. Incropera, F.P.; Dewitt, P.D.; Bergman, T.L.; Lavine, A.S.: *Fundamentals of Heat and Mass Transfer*. Wiley, New York (2006)
36. Yongsiri, K.; Eiamsa-ard, P.; Wongcharee, K.; Eiamsa-ard, S.: Augmented heat transfer in a turbulent channel flow with inclined detached-ribs. *Case Stud. Therm. Eng.* **3**, 1–10 (2014)
37. Singh, S.; Chander, S.; Saini, J.S.: Heat transfer and friction factor of discrete V-down rib roughness solar air heater ducts. *J. Renew. Sust. Energy* **3**, 013108 (2011)
38. Promvong, P.; Khanoknaiyakarn, C.; Kwankaomeng, S.; Thianpong, C.: Thermal behavior in solar air heater channel fitted with combined rib and delta-winglet. *Int. Commun. Heat Mass Transf.* **38**, 749–756 (2011)
39. Karwa, R.; Solanki, S.C.; Saini, J.S.: Thermo-hydraulic performance of solar air heaters having integral chamfered rib roughness on absorber plates. *Energy* **26**, 161–176 (2001)
40. Promvong, P.; Thianpong, C.: Thermal performance assessment of turbulent channel flows over different shaped ribs. *Int. Commun. Heat Mass Transf.* **35**, 1327–1334 (2008)

